Single-Shot Direct Tomography of the Complete Transverse Amplitude, Phase, and Polarization Structure of a Light Field

Ziyi Zhu,[1] Darrick Hay,[1] Yiyu Zhou,[2] Alexander Fyffe,[1] Brian Kantor,[1] Girish S. Agarwal,[3] Robert W. Boyd,[2,4] and Zhimin Shi[1,*]

[1] *Department of Physics, University of South Florida, Tampa, Florida 33620, USA*

[2] *The Institute of Optics, University of Rochester, Rochester, New York 14627, USA*

[3] *Institute for Quantum Science and Engineering, Department of Biological and Agricultural Engineering, and Department of Physics and Astronomy, Texas A&M University, TAMU4242, College Station, Texas 77843, USA*

[4] *Department of Physics, University of Ottawa, Ottawa, Ontario K1N 6N5, Canada*

(Received 10 October 2018; revised manuscript received 9 August 2019; published 18 September 2019)

We present a direct-tomography protocol that is capable of characterizing the transverse spatial profile of both the polarization and the complex amplitude of fully polarized vector light beams in a single-shot measurement. This protocol entails a sequence of steps: a coherent mode transformation, a weak polarization perturbation, and a polarization-resolved imaging process. The final readout is directly proportional to the complex-amplitude profile of the two polarization components of the vector beam. We experimentally demonstrate our direct measurement protocol on a variety of commonly used vector beams, including vector-vortex beams and full Poincaré beams. Our method provides the capability of acquiring all the information needed to characterize a fully polarized vector beam in a single-shot measurement. Such a real-time complete-tomography protocol has the potential to create new opportunities in emerging applications of vector beams as well as the fundamental study of complex physical systems with multiple degrees of freedom.

DOI: 10.1103/PhysRevApplied.12.034036

I. INTRODUCTION

Vector beams [1], characterized by their spatially varying polarization states, have recently garnered enormous interest in fundamental studies [2–4] and a wide spectrum of applications [5–12], due to the large amount of information that can be encoded within their transverse beam profiles. While there has been great success in generating vector beams using various methods [13–23], the densely coded information and inseparability between the spatial and polarization degrees of freedom present a challenge to the characterization of the complete field structure of vector beams. Conventional imaging polarimetry [24] only reveals the polarization profile of the beam, without providing any information on the transverse phase profile of each polarization component. Other methods [25,26] have characterized vector beams composed of a limited number of selected modes, but since the selected modes typically do not span a complete mode basis set, these methods are incapable of fully describing the transverse profile of an arbitrary vector beam. In addition, most available optical-phase measurement techniques [27], including Shack-Hartmann microlens arrays and interferometric techniques, are designed for scalar beams and cannot easily reveal the phase structure of vector beams, nor their polarization profiles. The lack of a complete beam-metrology technique for vector beams has hampered the broader impact of vector fields in many important applications [8], including polarization-resolved imaging through tissues [12,28], free-space communication through turbulence [11,29,30], quantum-information encryption [31], surveillance, and sensing [32].

In this work, we describe a scan-free direct-tomography protocol that is capable of characterizing the complete transverse-field structure of a fully polarized vector beam in a single measurement. Our tomographic characterization process involves a coherent mode transformation, a weak polarization perturbation, also known as "weak measurement" [33–39], and a measurement of the polarization profile of the final perturbed field. Through such a protocol, our measurement result is directly related to the complex-amplitude profile of both polarization components of the vector beam, from which the full spatial-polarization profile of the vector beam can be retrieved in a straightforward fashion. We demonstrate the single-shot characterization capability of our direct-tomography protocol by measuring the complete field structure of a variety of vector beams that are important for critical applications. We highlight the

*zhiminshi@usf.edu

unique capability of our method as compared to existing technologies by distinguishing vector beams that have different polarization profiles but identical complex-field profiles for each polarization component and beams that have identical polarization profiles but different complex-field profiles in each polarization component. The consistent high fidelity in all of our measurements demonstrates the robust and versatile nature of our approach, which can help to enable a wide spectrum of the aforementioned emerging applications of vector beams. Furthermore, our concept can also be extended toward the development of metrology techniques for other complex physical systems with multiple degrees of freedom.

II. THEORETICAL FRAMEWORK

A fully polarized vector beam can be expressed as the coherent superposition of two scalar beams with orthogonal polarizations as follows:

$$\vec{\mathbf{E}}(u,v) = \hat{e}_l E_l(u,v) + \hat{e}_r E_r(u,v), \tag{1}$$

where $\hat{e}_l$ and $\hat{e}_r$ denote the unit vectors in the left- and right-handed circular-polarization (LCP and RCP) bases, respectively, and $E_l(u,v)$ and $E_r(u,v)$ denote the transverse complex-amplitude profiles of the two circular-polarization components, respectively. Note that the vector beam can also be expressed in any other polarization basis.

To characterize such a vector beam, our direct-tomography protocol comprises three main steps, as illustrated in Fig. 1. We first apply a relative transverse displacement of $2\delta u$ between the two polarization components of the vector beam, followed by separate polarization adjustment so that the two polarization components are adjusted into the same polarization state. As a result, the vector beam is first transformed into a fully coherent scalar beam with two transversely separated parts corresponding to the two polarization components of the vector beam, as

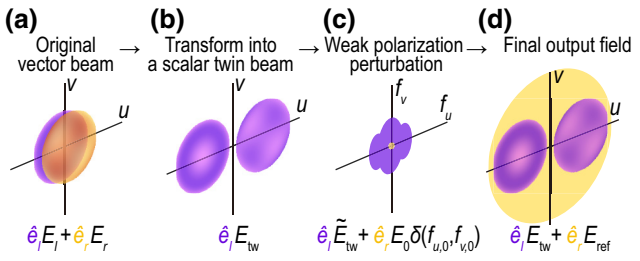

FIG. 1. An illustration of the three-step procedure of the direct-tomography protocol for vector beams: the polarization components are spatially separated and adjusted into a twin beam; a weak polarization perturbation is applied in the Fourier domain of the twin beam; and polarization-resolved imaging is performed on the final output field.

follows:

$$\hat{e}_l E_{tw}(u,v) = \hat{e}_l \left[E_l(u+\delta u, v) + E_r(u-\delta u, v)\right]. \tag{2}$$

For convenience, we refer to this transformed scalar beam as the "twin beam." Next, we perform a weak polarization perturbation, also known as the "weak measurement," on one specific Fourier component of the twin beam. The field in the Fourier plane after such a polarization perturbation can be expressed as follows:

$$\begin{aligned}\tilde{\vec{\mathbf{E}}}_{pert}(f_u,f_v) &= \hat{e}_l \tilde{E}_{tw}(f_u,f_v)[1+(\cos\alpha - 1)\delta(f_{u,0},f_{v,0})] \\ &\quad + \hat{e}_r \tilde{E}_{tw}(f_u,f_v)(\sin\alpha)\delta(f_{u,0},f_{v,0}) \\ &\approx \hat{e}_l \tilde{E}_{tw}(f_u,f_v) + \hat{e}_r E_0 \delta(f_{u,0},f_{v,0}),\end{aligned} \tag{3}$$

where $\tilde{E}_{tw}(f_u,f_v) = \mathcal{F}E_{tw}(u,v)$ is the twin beam expressed in its Fourier plane, α denotes the strength of the polarization perturbation in terms of a rotation angle, $\delta(f_{u,0},f_{v,0})$ is the Dirac delta function centered at $(f_{u,0},f_{v,0})$ in the Fourier plane of the twin beam, and $E_0 = \alpha\tilde{E}_{tw}(f_{u,0},f_{v,0})$ denotes the amplitude of the orthogonally polarized pointlike field. One sees that when the strength of the polarization perturbation α is small, the field in the original left-handed circular polarization is maintained to the first-order approximation and yet a pointlike field in the orthogonal polarization is generated in the Fourier plane.

We then take an inverse Fourier transform on the perturbed beam and measure the spatial-polarization profile of the weakly perturbed twin-beam field in the u-v plane, which can be expressed as follows:

$$\vec{\mathbf{E}}_{det}(u,v) \approx \hat{e}_l E_{tw}(u,v) + \hat{e}_r E_{ref}, \tag{4}$$

where E_{ref} is a well-defined plane wave resulting from the polarization perturbation applied as a delta function in the Fourier plane. It can be shown that the spatial-polarization profile of the final output field $\vec{\mathbf{E}}_{det}(u,v)$ is directly proportional to the complex amplitude of the scalar twin-beam field $E_{tw}(u,v)$, i.e., that of the two polarization components, $E_l(u,v)$ and $E_r(u,v)$, of the vector beam. For example, if the scalar twin-beam field $E_{tw}(u,v)$ before polarization perturbation is set to be left-handed circularly polarized, its complex-field profile can be expressed as follows:

$$E_{tw}(u,v) \propto S_{1,det}(u,v) - iS_{2,det}(u,v), \tag{5}$$

where $S_{1,det}(u,v)$ and $S_{2,det}(u,v)$ are the Stokes-parameter profiles describing the projected polarization profile of the weakly perturbed twin beam in the horizontal-vertical and diagonal-antidiagonal linear polarization bases, respectively. Since the complex-amplitude profiles of both polarization components $E_l(u,v)$ and $E_r(u,v)$ are measured coherently, one can consequently obtain the polarization

profile of the vector beam. As a result, the complete field structure of the vector beam is determined in a single shot through such a direct-tomography procedure. A detailed description of our theoretical framework is provided in the Supplemental Material [40].

III. EXPERIMENTAL CONFIGURATION

To demonstrate our direct measurement protocol for vector beams, we construct an experimental setup as illustrated in Fig. 2, which includes a vector-beam-generation module and a direct-tomography characterization module. We start with an expanded and collimated laser beam at 532 nm and use a spatial light modulator (SLM), a $4f$ imaging system and a Sagnac interferometer to generate vector beams of arbitrary field structure [41–43].

In the direct-tomography module, a second Sagnac interferometer is used to convert the vector beam to a scalar twin beam. The field then propagates through a second $4f$ imaging system, where the Fourier transform of the beam is accessed at the focal plane of the $4f$ imaging system and the output field is measured at the image plane. A weak polarization perturbation is applied on the focal plane using a second polarization-sensitive phase-only SLM. The size of the perturbation area on the SLM is chosen to be comparable to the diffraction-limited spot size of the $4f$ system and the polarization alteration is small enough to satisfy the weak perturbation condition. Finally, the spatial-polarization profile of the perturbed field at the image plane, which contains the information about the complete field structure of the vector beam, is measured using a polarization-resolving camera in a single shot. More details of our experimental procedure are given in the Supplemental Material [40].

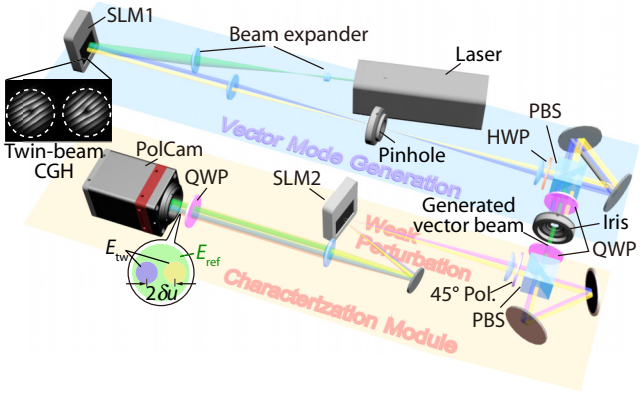

FIG. 2. A schematic diagram of the experimental setup, which includes a vector-beam-generation module and a direct-measurement module: CGH, computer-generated hologram; SLM, spatial light modulator; Pol., polarizer; PBS, polarizing beam splitter; HWP, half-wave plate; PolCam, polarization-resolving camera; QWP, quarter-wave plate.

Note that both the theoretical framework and the experimental apparatus outlined here can be directly applied to the measurement of quantum states of light using identically prepared single photons, provided that we use detector arrays that are capable of detecting single photons with high quantum efficiency, such as single-photon avalanche diode (SPAD) arrays, electron-multiplying charge-coupled-device (CCD) cameras, and intensified CCD cameras. Note also that the limited quantum efficiency of single-photon detector arrays would require summing over a large number of measurements using our protocol on identically prepared single photons to average out the readout noise, but the complex-valued state vector of single photons in the position-polarization Hilbert space can still be measured directly using a single experimental setup, without the need of any reconfiguration or scanning procedure.

IV. EXPERIMENTAL DEMONSTRATIONS

Using this setup, we generate and measure a variety of vector beams, including several that are widely used in many applications. To quantitatively evaluate our direct-tomography result, we define a "vector-beam fidelity" as the figure of merit, which is expressed as follows:

$$\mathcal{F} \equiv \frac{\left|\sum_p \int E_{p,\mathrm{exp}}(u,v) E^*_{p,\mathrm{the}}(u,v)\, du\, dv\right|}{\sqrt{\sum_p \int \left|E_{p,\mathrm{exp}}(u,v)\right|^2 du\, dv}\sqrt{\sum_p \int \left|E_{p,\mathrm{the}}(u,v)\right|^2 du\, dv}}, \tag{6}$$

where the subscript p denotes the polarization components under the chosen basis and $E_{p,\mathrm{exp}}$ and $E_{p,\mathrm{the}}$ denote the measured results and theoretical predictions, respectively. Such a figure of merit not only reflects the measurement accuracy of the complex-valued field amplitude of each polarization component, but it is also sensitive to the relative phase of the two polarization components, which reflects the measurement accuracy of the spatial-polarization profiles of the vector beams.

First, we generate a vector beam that has uniform amplitude over a circular aperture and two different Zernike polynomial phase profiles, Z_4^2 and Z_2^{-2}, encoded into the LCP and RCP components, respectively. The directly measured real and imaginary parts of the two circular-polarization components are shown in Figs. 3(a)–3(d). The corresponding phase profiles of the two polarization components as well as the profiles of three normalized Stokes parameters are shown in Figs. 3(e)–3(i), respectively. One sees that our experimental results match well with the theoretical expectations, shown as insets in the upper-right corner of each plot.

The fidelity of our measurement on the Zernike vector beam shown in Fig. 3 is approximately 0.95 and similar high fidelity is observed for a series of tested vector beams

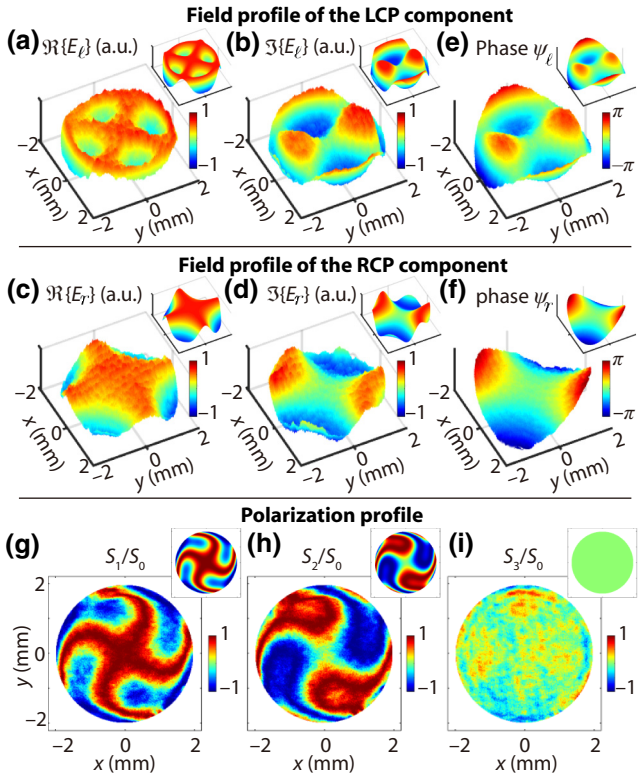

FIG. 3. (a)–(d) The directly measured real and imaginary parts of the left- and right-handed circular-polarization components of a vector beam that has uniform amplitude over a circular aperture and Zernike polynomial Z_4^2 and Z_2^{-2} phase profiles; (e),(f) the corresponding phase profiles of the two polarization components; (g)–(i) the corresponding normalized Stokes parameters of the vector beam. The insets in the upper-right corners are theoretical predictions.

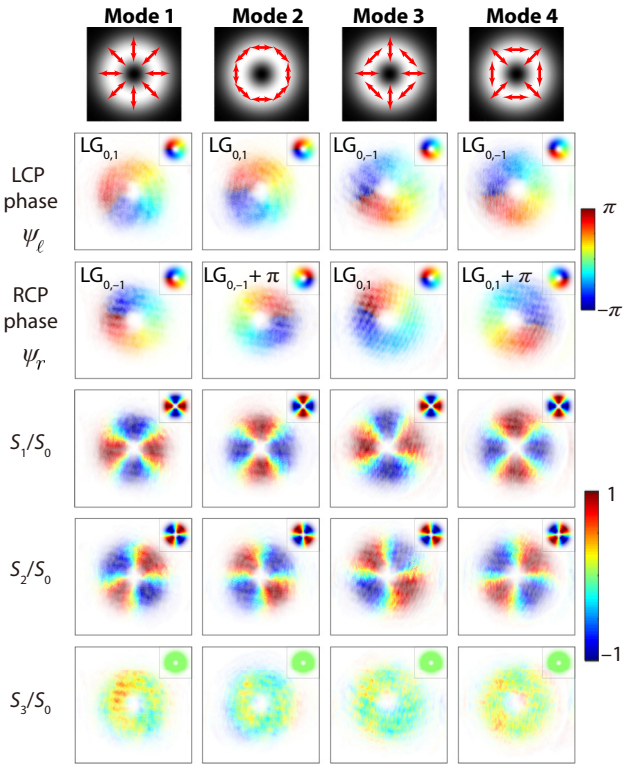

FIG. 4. The measured phase of the two polarization components and the normalized Stokes parameters of four vector-vortex beams that are commonly used for high-dimensional optical communication. These vector-vortex beams are comprised of $LG_{0,1}$ and $LG_{0,-1}$ Laguerre-Gaussian beams as the polarization components, with differing relative phase differences. The color saturation reflects the beam intensity. The insets in the upper-right corners are theoretical predictions.

with different Zernike phase profiles. The high fidelity of our results demonstrates that our technique is capable of accurately measuring the full complete field structure of vector beams. The total number of effective pixels of our experimental result is approximately 100 000, being limited by the numerical aperture and the field of view of the imaging system and by the pixel density of the camera used in the experiment.

Second, we measure a family of four vector-vortex beams [1] that are being widely used for high-dimensional secure quantum communication [44–46]. These four vector-vortex beams use $LG_{0,1}$ and $LG_{0,-1}$ Laguerre-Gaussian (LG) modes as the two circular-polarization components, with a relative phase difference of 0 or π. Here, $LG_{p,l}$ denotes the Laguerre-Gaussian mode with radial index p and azimuthal index l. As a result, these four vector beams have identical intensity profiles but completely different polarization profiles, as illustrated in the first row in Fig. 4. Since these four vector modes are orthogonal to each other, they can be used to represent two bits of information in a spatial-mode encoding protocol. As shown in the second and third rows in Fig. 4, our direct-tomography technique accurately reveals the azimuthal phase profile of each LG mode, as well as the donut-shaped amplitude profile (illustrated by the saturation of each plot). Moreover, modes 1 and 2 (the same for modes 3 and 4) have identical transverse phase profiles for the LCP and RCP components, but the relative phase between the LCP and RCP components is 0 and π, respectively. This relative phase difference determines that mode 1 is radially polarized and mode 2 is azimuthally polarized. As shown in Fig. 4, our direct-tomography method correctly captures the relative phase difference between the two polarization components for each mode, which consequently reveals the correct polarization profiles. Such accurate mapping of the Stokes parameters is not possible if the complex-field profiles of the two polarization components are measured individually. The fidelity values of our measurement results for the four vector-vortex beams are 0.91, 0.92, 0.92, and 0.94, respectively.

To further emphasize the advantage of our direct-tomography protocols over conventional imaging

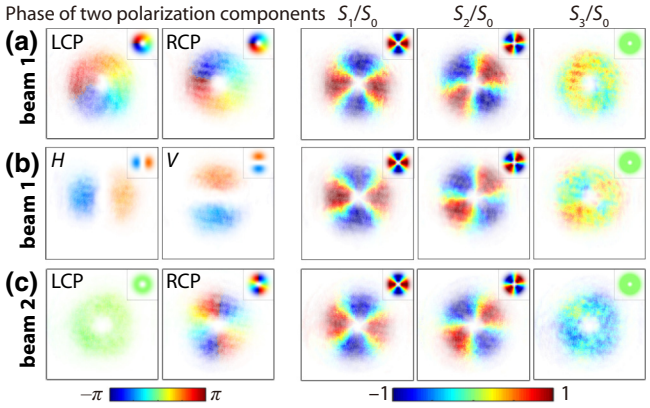

FIG. 5. The measured phase of the two polarization components and the normalized Stokes parameters of: (a) a vector-vortex beam comprised of $LG_{0,1}$ and $LG_{0,-1}$ Laguerre-Gaussian modes as two circular-polarization components; (b) the same beam measured in the horizontal and vertical polarization bases; and (c) a different beam that has identical polarization profiles but different phase profiles for the two polarization components. The color saturation reflects the beam intensity. The insets in the upper-right corners are theoretical predictions.

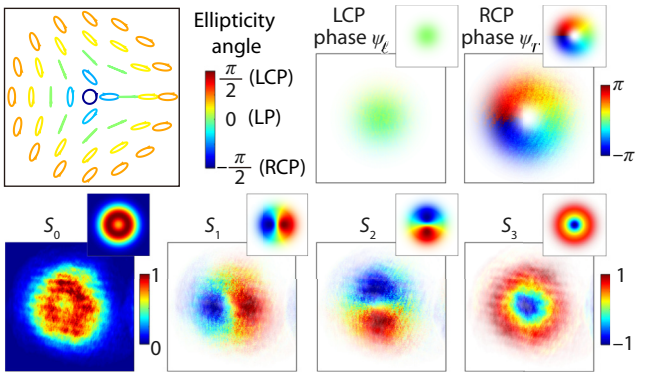

FIG. 6. The measured phase profile of the two circular-polarization components and the Stokes profiles of a full Poincaré beam: LP, linear polarization. The color saturation reflects the beam intensity. The theoretical polarization profile of this beam is illustrated in the upper-left corner of the figure and the insets in the upper-right corners are theoretical predictions of each profile.

polarimetry, we next demonstrate their ability to distinguish between two different vector beams with identical polarization profiles. The first beam is the radially polarized vector-vortex beam comprised of $LG_{0,1}$ and $LG_{0,-1}$ Laguerre-Gaussian modes in the circular-polarization bases shown as mode 1 in Fig. 4. Besides the accurate characterization of the complete field structure in the circular-polarization basis as shown in Fig. 5(a), we also measure the beam in the horizontal-vertical (H-V) linear polarization basis by removing the QWP at the very front of the characterization module. As shown in Fig. 5(b), our experimental results match well with the theoretical prediction of the $HG_{1,0}$ and $HG_{0,1}$ Hermite-Gaussian (HG) modes [1], illustrating the versatility of our direct-tomography method in characterizing vector beams in arbitrary polarization bases. The second vector beam is created using the same amplitude profile as the first beam, but we remove the spiral phase from the LCP component and double the spiral phase on the RCP component. Since the relative phase difference between the LCP and RCP components at each spatial point remains the same, these two vector beams have identical polarization profiles and therefore are indistinguishable if measured by conventional imaging polarimetry. As shown in Figs. 5(a) and 5(c), our measurement results not only show the polarization indistinguishability of the two vector beams but also accurately reveal the different phase profiles of the two beams in each polarization component. The capability of resolving the complex-field profile of individual polarization components makes our direct-tomography protocol a more valuable tool as compared to conventional imaging polarimetry.

Finally, we demonstrate the generation and characterization of a full Poincaré beam, which has attracted a lot of research interest for its richness in fundamental physics as well as its potential applications in imaging and particle tracking [47,48]. Our full-Poincaré beam is generated by superposing an LCP fundamental Gaussian mode and an RCP $LG_{0,1}$ Laguerre-Gaussian mode. As shown in Fig. 6, our experimental results match well with the theoretical predictions (shown as insets in the upper-right corner of each plot), which indicates that the polarization state across the beam indeed spans the entire surface of the polarization Poincaré sphere. The fidelity of our measurement result is 0.95, which further demonstrates that our direct-tomography method is capable of characterizing vector beams with any possible field structure. Note also that a complete knowledge of the transverse-field structure of the vector beam at one plane could also reveal the evolution of its full transverse-field structure as the vector beam travels through free space or a well-described optical system through the application of well-known Fourier optics methods. Such a capability could reveal, e.g., the spatial evolution of critical polarization points of the vector fields [4] through a single-shot measurement, rather than it being necessary to perform polarization measurements plane by plane using conventional imaging polarimetry.

V. CONCLUSION

In summary, we introduce a direct-tomography protocol that is capable of characterizing the complete transverse-field profile of fully polarized vector beams in a single-shot measurement. The tomographic characterization process involves a separation of orthogonal polarization components, a weak polarization perturbation, and a measurement of the polarization profile of the perturbed field. We

show that our final measurement result is directly related to the complex-amplitude profile of the two orthogonal polarization components of the vector beam, from which the spatial polarization profile of the vector beam can be calculated in a straightforward fashion. We demonstrate our direct-tomography protocol by measuring a variety of vector beams that are important to optical information science, including vector-vortex beams and full Poincaré beams. No signal averaging is used for any of the experimental results presented here. Our experimental results show consistently high data fidelity and the capability of revealing both the complex amplitude and the polarization structure in a single-shot measurement provides a robust and versatile metrology tool in real time for fundamental studies of vector beams and a wide spectrum of applications utilizing vector beams. Our approach can also be extended to the development of metrology protocols for other complex physical systems with multiple degrees of freedom.

ACKNOWLEDGMENTS

Z.Z., D.H., Y.Z., A.F., B.K., R.W.B., and Z.S. acknowledge support from ONR Grant No. N00014-17-1-2443. G.S.A. acknowledges support from the Welch Grant Award No. A-1943-20180324. Z.S. acknowledges helpful discussions with Q. Zhan. R.W.B. acknowledges useful discussions with J. Lundeen and funding from the Natural Sciences and Engineering Research Council of Canada, the Canada Research Chairs program, and the Canada First Research Excellence Fund award on Transformative Quantum Technologies.

[1] Q. Zhan, Cylindrical vector beams: From mathematical concepts to applications, Adv. Opt. Photon. **1**, 1 (2009).
[2] K. H. Kagalwala, G. Di Giuseppe, A. F. Abouraddy, and B. E. A. Saleh, Bell's measure in classical optical coherence, Nat. Photonics **7**, 72 (2013).
[3] T. Bauer, P. Banzer, E. Karimi, S. Orlov, A. Rubano, L. Marrucci, E. Santamato, R. W. Boyd, and G. Leuchs, Observation of optical polarization Möbius strips, Science **347**, 964 (2015).
[4] H. Larocque, D. Sugic, D. Mortimer, A. J. Taylor, R. Fickler, R. W. Boyd, M. R. Dennis, and E. Karimi, Reconstructing the topology of optical polarization knots, Nat. Phys. **14**, 1079 (2018).
[5] A. F. Abouraddy and K. C. Toussaint, Three-Dimensional Polarization Control in Microscopy, Phys. Rev. Lett. **96**, 153901 (2006).
[6] Q. Zhan and J. R. Leger, Focus shaping using cylindrical vector beams, Opt. Express **10**, 324 (2002).
[7] M. G. Donato, S. Vasi, R. Sayed, P. H. Jones, F. Bonaccorso, A. C. Ferrari, P. G. Gucciardi, and O. M. Maragò, Optical trapping of nanotubes with cylindrical vector beams, Opt. Lett. **37**, 3381 (2012).
[8] H. Rubinsztein-Dunlop *et al.*, Roadmap on structured light, J. Opt. **19**, 013001 (2017).
[9] M. Beresna, M. Gecevičius, and P. G. Kazansky, Polarization sensitive elements fabricated by femtosecond laser nanostructuring of glass, Opt. Mater. Express **1**, 783 (2011).
[10] E. Otte, C. Rosales-Guzmán, B. Ndagano, C. Denz, and A. Forbes, Entanglement beating in free space through spin-orbit coupling, Light Sci. Appl. **7**, 18009 (2018).
[11] B. Ndagano, B. Perez-Garcia, F. S. Roux, M. McLaren, C. Rosales-Guzman, Y. Zhang, O. Mouane, R. I. Hernandez-Aranda, T. Konrad, and A. Forbes, Characterizing quantum channels with non-separable states of classical light, Nat. Phys. **13**, 397 (2017).
[12] H. B. de Aguiar, S. Gigan, and S. Brasselet, Polarization recovery through scattering media, Sci. Adv. **3**, e1600743 (2017).
[13] C. Maurer, A. Jesacher, S. Fürhapter, S. Bernet, and M. Ritsch-Marte, Tailoring of arbitrary optical vector beams, New J. Phys. **9**, 78 (2007).
[14] X.-L. Wang, J. Ding, W.-J. Ni, C.-S. Guo, and H.-T. Wang, Generation of arbitrary vector beams with a spatial light modulator and a common path interferometric arrangement, Opt. Lett. **32**, 3549 (2007).
[15] L. Marrucci, C. Manzo, and D. Paparo, Optical Spin-to-Orbital Angular Momentum Conversion in Inhomogeneous Anisotropic Media, Phys. Rev. Lett. **96**, 163905 (2006).
[16] S. Slussarenko, A. Murauski, T. Du, V. Chigrinov, L. Marrucci, and E. Santamato, Tunable liquid crystal q-plates with arbitrary topological charge, Opt. Express **19**, 4085 (2011).
[17] F. Cardano, E. Karimi, S. Slussarenko, L. Marrucci, C. de Lisio, and E. Santamato, Polarization pattern of vector vortex beams generated by q-plates with different topological charges, Appl. Opt. **51**, C1 (2012).
[18] G. Volpe and D. Petrov, Generation of cylindrical vector beams with few-mode fibers excited by Laguerre-Gaussian beams, Opt. Commun. **237**, 89 (2004).
[19] S. Ramachandran, P. Kristensen, and M. F. Yan, Generation and propagation of radially polarized beams in optical fibers, Opt. Lett. **34**, 2525 (2009).
[20] N. Radwell, R. Hawley, J. Götte, and S. Franke-Arnold, Achromatic vector vortex beams from a glass cone, Nat. Commun. **7**, 10564 (2016).
[21] Z. Zhao, J. Wang, S. Li, and A. E. Willner, Metamaterials-based broadband generation of orbital angular momentum carrying vector beams, Opt. Lett. **38**, 932 (2013).
[22] E. Karimi, S. A. Schulz, I. D. Leon, H. Qassim, J. Upham, and R. W. Boyd, Generating optical orbital angular momentum at visible wavelengths using a plasmonic metasurface, Light Sci. Appl. **3**, e167 (2014).
[23] A. Arbabi, Y. Horie, M. Bagheri, and A. Faraon, Dielectric metasurfaces for complete control of phase and polarization with subwavelength spatial resolution and high transmission, Nat. Nanotechnol. **10**, 937 (2015).
[24] J. S. Tyo, D. L. Goldstein, D. B. Chenault, and J. A. Shaw, Review of passive imaging polarimetry for remote sensing applications, Appl. Opt. **45**, 5453 (2006).
[25] B. Ndagano, I. Nape, B. Perez-Garcia, S. Scholes, R. I. Hernandez-Aranda, T. Konrad, M. P. Lavery, and A. Forbes, A deterministic detector for vector vortex states, Sci. Rep. **7**, 13882 (2017).

[26] M. McLaren, T. Konrad, and A. Forbes, Measuring the nonseparability of vector vortex beams, Phys. Rev. A **92**, 023833 (2015).
[27] D. Malacara, *Optical Shop Testing* (John Wiley & Sons, Hoboken, 2007).
[28] J. M. Brockman, A. T. Blanchard, V. P.-Y. Ma, W. D. Derricotte, Y. Zhang, M. E. Fay, W. A. Lam, F. A. Evangelista, A. L. Mattheyses, and K. Salaita, Mapping the 3D orientation of piconewton integrin traction forces, Nat. Methods **15**, 115 (2018).
[29] W. Cheng, J. W. Haus, and Q. Zhan, Propagation of vector vortex beams through a turbulent atmosphere, Opt. Express **17**, 17829 (2009).
[30] M. A. Cox, C. Rosales-Guzmán, M. P. J. Lavery, D. J. Versfeld, and A. Forbes, On the resilience of scalar and vector vortex modes in turbulence, Opt. Express **24**, 18105 (2016).
[31] A. Sit, F. Bouchard, R. Fickler, J. Gagnon-Bischoff, H. Larocque, K. Heshami, D. Elser, C. Peuntinger, K. Günthner, B. Heim, C. Marquardt, G. Leuchs, R. W. Boyd, and E. Karimi, High-dimensional intracity quantum cryptography with structured photons, Optica **4**, 1006 (2017).
[32] S. Berg-Johansen, F. Töppel, B. Stiller, P. Banzer, M. Ornigotti, E. Giacobino, G. Leuchs, A. Aiello, and C. Marquardt, Classically entangled optical beams for high-speed kinematic sensing, Optica **2**, 864 (2015).
[33] J. S. Lundeen, B. Sutherland, A. Patel, C. Stewart, and C. Bamber, Direct measurement of the quantum wavefunction, Nature **474**, 188 (2011).
[34] J. S. Lundeen and C. Bamber, Procedure for Direct Measurement of General Quantum States Using Weak Measurement, Phys. Rev. Lett. **108**, 070402 (2012).
[35] S. Wu, State tomography via weak measurements, Sci. Rep. **3**, 1193 (2013).
[36] M. Mirhosseini, O. S. Maga na Loaiza, S. M. Hashemi Rafsanjani, and R. W. Boyd, Compressive Direct Measurement of the Quantum Wave Function, Phys. Rev. Lett. **113**, 090402 (2014).
[37] J. Z. Salvail, M. Agnew, A. S. Johnson, E. Bolduc, J. Leach, and R. W. Boyd, Full characterization of polarization states of light via direct measurement, Nat. Photonics **7**, 316 (2013).
[38] M. Malik, M. Mirhosseini, M. P. Lavery, J. Leach, M. J. Padgett, and R. W. Boyd, Direct measurement of a 27-dimensional orbital-angular-momentum state vector, Nat. Commun. **5**, 3115 (2014).
[39] Z. Shi, M. Mirhosseini, J. Margiewicz, M. Malik, F. Rivera, Z. Zhu, and R. W. Boyd, Scan-free direct measurement of an extremely high-dimensional photonic state, Optica **2**, 388 (2015).
[40] See the Supplemental Material at http://link.aps.org/supplemental/10.1103/PhysRevApplied.12.034036 for detailed descriptions of the theoretical framework of the direct tomography protocol as well as the experimental procedures.
[41] B. Perez-Garcia, C. López-Mariscal, R. I. Hernandez-Aranda, and J. C. Gutiérrez-Vega, On-demand tailored vector beams, Appl. Opt. **56**, 6967 (2017).
[42] J. A. Davis, D. M. Cottrell, J. Campos, M. J. Yzuel, and I. Moreno, Encoding amplitude information onto phase-only filters, Appl. Opt. **38**, 5004 (1999).
[43] V. Arrizón, U. Ruiz, R. Carrada, and L. A. González, Pixelated phase computer holograms for the accurate encoding of scalar complex fields, J. Opt. Soc. Am. A **24**, 3500 (2007).
[44] G. Milione, T. A. Nguyen, J. Leach, D. A. Nolan, and R. R. Alfano, Using the nonseparability of vector beams to encode information for optical communication, Opt. Lett. **40**, 4887 (2015).
[45] G. Milione, M. P. J. Lavery, H. Huang, Y. Ren, G. Xie, T. A. Nguyen, E. Karimi, L. Marrucci, D. A. Nolan, R. R. Alfano, and A. E. Willner, 4×20 Gbit/s mode division multiplexing over free space using vector modes and a q-plate mode (de)multiplexer, Opt. Lett. **40**, 1980 (2015).
[46] A. Sit, F. Bouchard, R. Fickler, J. Gagnon-Bischoff, H. Larocque, K. Heshami, D. Elser, C. Peuntinger, K. Günthner, B. Heim, C. Marquardt, G. Leuchs, R. W. Boyd, and E. Karimi, High-dimensional intracity quantum cryptography with structured photons, Optica **4**, 1006 (2017).
[47] A. M. Beckley, T. G. Brown, and M. A. Alonso, Full Poincaré beams, Opt. Express **18**, 10777 (2010).
[48] D. Naidoo, F. S. Roux, A. Dudley, I. Litvin, B. Piccirillo, L. Marrucci, and A. Forbes, Controlled generation of higher-order Poincaré sphere beams from a laser, Nat. Photonics **10**, 327 (2016).